2-15-2023

# Periodicities and Plasma Density Structure of Jupiter's Dawnside Magnetosphere

Xuanye Ma
*Embry-Riddle Aeronautical University*, max@erau.edu

A.A. Schok
*University of Alaska, Fairbanks*

P.A. Delamere
*University of Alaska, Fairbanks*

B. Mino
*University of Alaska, Fairbanks*

P.A. Damiano
*University of Alaska, Fairbanks*

*See next page for additional authors*

## Authors

Xuanye Ma, A.A. Schok, P.A. Delamere, B. Mino, P.A. Damiano, B. Zhang, and A. Sciola

# Periodicities and plasma density structure of Jupiter's dawnside magnetosphere

**A. A. Schok[1], P. A. Delamere[1], B. Mino[1], P. A. Damiano[1], B. Zhang[2], A. Sciola[3], K. Sorathia[3], S. Wing[3], J. R. Johnson[4], X. Ma[5], Z. Yao[6], O. Brambles[7]**

[1]Geophysical Institute, University of Alaska Fairbanks, Fairbanks, AK, USA,
[2]University of Hong Kong, Hong Kong SAR, China
[3]Applied Physics Laboratory, The Johns Hopkins University, Laurel, MD, USA
[4]Andrews University, Berrien Springs, MI, USA
[5]Embry-Riddle Aeronautical University, Daytona Beach, FL, USA
[6]University of Chinese Academy of Sciences, Beijing, China
[7]O.J. Brambles Consulting, Preston, UK

## Key Points:

- Three-regions with different plasma confinement characteristics have been identified in Jupiter's dawn to post-midnight magnetosphere.
- Comparison of Juno data and GAMERA simulations suggest a very structured plasmadisc.
- Periodicities in the one to four hour range could be related to plasmadisc structure.

Corresponding author: =name=, `=email address=`

**Abstract**

The ability to quantify variations in magnetic field topology and density within Jupiter's magnetosphere is an important step in understanding the overall structure and dynamics. The Juno spacecraft has provided a rich data set in the dawnside magnetosphere. The recent Grid Agnostic MHD for Extended Research Applications (GAMERA) global simulation study by Zhang et al. (2021) showed a highly structured plasmadisc with closed magnetic field lines mapping between the outer dawn-tail flank and the high-latitude polar region. To test these model predictions, we examined Juno's magnetic field data and electron/energetic particle data to categorize portions of orbits 1-15 into one of three regions based on plasma confinement: the flux pileup region, the intermediate region, and the plasmadisc region. For each region we examined periodicities from magnetic field fluctuations and particle density fluctuations on the 1-10 hours time scale. Periodicities on this time scale could relate to internal (e.g. plasmadisc structure) or external processes (e.g. Kelvin-Helmholtz vortices). Similar analysis was performed on the GAMERA simulation with the data split into two regions, an outer ($150 > R > 60$) region and an inner ($R < 60$) region. Finally, using published density moments from Huscher et al. (2021) we compared the relative density variations of the Juno moments and the GAMERA simulation to further understand the overall structure and dynamics of the plasmadisc. The agreement between data and simulation supports the existence of such a highly structured plasmadisc.

# Plain Language Summary

A very complex and poorly understood problem of Jupiter is the structure and dynamics of the planet's space environment (i.e., "magnetosphere"), due to its sheer size and unique internal ionized gas (i.e., plasma) sourced from the moon, Io. Thanks to the Juno mission we are able to analyze data from previously unexplored regions around the planet. It has been demonstrated, using Voyager data, that ionized gas from Io formed a plasma disc-like structure around the planet in the equatorial plane, becoming less confined in the outer regions. Computer simulations showed a similar structure. In order to investigate this structure we utilized magnetic field data and particle data from the Juno spacecraft. This data was analyzed to understand the occurrence of regular fluctuations in the magnetic field and gas density, and to understand the spatial domains where regular fluctuations occur. Similar analysis was done on magnetic field and density data from simulations for comparison. We found relations between the Juno data and simulation data that suggest a much more variable and structured plasma disc as well as a region in the dawn/tail flank that is magnetically connected to the high latitude polar region.

# 1 Introduction

Jupiter's dawnside outer magnetosphere can be characterized as a battleground between internally-driven sunward flow and solar wind-driven tailward flow, leading to a highly variable and poorly understood region of the magnetosphere. Prior to the Pioneer spacecraft encounters, the "planetary wind" model was proposed, whereby centrifugal stresses dominate when flows exceed the local Alfvén speed (Kennel & Coroniti, 1977). A key aspect of this model is the generation of internal shocks, an abrupt breakdown in corotation, and radial outflow of plasma. The planetary wind model was not supported by Voyager observations, which instead showed persistent corotation and no internal shocks. Following the Voyager 1 flyby, an extended region along the dawn flank was characterized as a "boundary layer" or "magnetospheric wind" that was distinctly different from the equatorially confined magnetodisc (Gurnett et al., 1980; Krimigis et al., 1979). Vasyliunas (1983) developed a model for internal magnetic reconnection (also known as the "Vasyliunas cycle") that included an extended x-line in the dawn/tail region. The Vasyliunas cycle accounted for conservation of magnetic flux, a dawn flank "magnetospheric wind" and tail plasma composition similar to the inner magnetosphere. A further analysis of the Voyager 2 energetic particle data led Cheng and Krimigis (1989) to augment the global convection models by introducing three distinct regions of the magnetosphere: 1) an inner heavy-ion-rich region, 2) a cross tail flow region with significant solar wind composition (presumably transported into the magnetosphere in the dusk sector), and 3) magnetospheric wind region with heavy-ion-rich composition. The boundary between regions 1) and 2) for Voyager 2 was at roughly 60 $R_J$.

An additional feature of the dawnside outer magnetosphere is the so-called "cushion region" (Kivelson & Southwood, 2005; Gershman et al., 2018). Observations of the prenoon sector by Pioneer, Voyager, Ulysses, and Galileo spacecraft showed a more dipolar magnetic field topology that lacked a clear 10-hour periodicity. Kivelson and Southwood (2005) suggested that the cushion was composed of empty flux tubes from the tail. Delamere and Bagenal (2010) argued that the cushion should be similar to the Gurnett et al. (1980) boundary layer, encompassing 10s of $R_J$ adjacent to the magnetopause boundary and used the terminology "cushion/interaction region". However, in an initial assessment of Juno data, Gershman et al. (2018) found no evidence for a cushion region in the dawn/tail region and argued that the cushion is formed by the gradual compression of the magnetic field corotating to the dayside. A similar ambiguity exists for Saturn's cushion region where Staniland et al. (2021) showed that the cushion forms rarely at Saturn and to add confusion to the issue, Delamere et al. (2015) defined the cushion as a region where the $B_\theta$ component exceeds the dipole field strength, which is a common property for the giant magnetospheres.

Following Voyager, it was widely understood that Jupiter's magnetosphere was largely open based on wave data and energetic particle observations. Voyager 2 electric field measurements showed spectra outside of the magnetodisc to be similar to solar wind spectra (Gurnett et al., 1980). These regions were referred to as the "tail lobe" (i.e., by terrestrial analogue, the lobes are open field lines). Khurana et al. (2004) illustrated a dawn/dusk asymmetry with much of the dawnside magnetosphere containing open flux. However, McComas and Bagenal (2007), McComas and Bagenal (2008) and Delamere and Bagenal (2010) argued instead for a largely closed magnetosphere due, in part, to the preponderance of auroral activity in the polar regions (Grodent, 2014). To further illustrate the open/closed conundrum posed by energetic particle data, Delamere and Bagenal (2010) compiled observations from Pioneer, Voyager, Ulysses, and New Horizons and categorized the data with elevated magnetospheric count rates or background solar wind count rates. Using the Khurana and Tsyganenko (2002) magnetic field model, the observation point was mapped to the equatorial plane. The solar wind count rates mapped (roughly) in the dawnside magnetosphere to a region beyond 60 $R_J$. Delamere and Bagenal (2010) concluded that an intermittent reconnection process must exist on these field lines that must, somehow, be associated with large-scale Kelvin-Helmholtz activity on the magnetopause boundary in the case of a largely closed magnetosphere.

One of the major new results from Juno observations is evidence of a largely closed magnetosphere. Szalay et al. (2022) demonstrated that Jupiter's extreme high latitude polar regions contain magnetospheric heavy ions with energy spectra that is consistent with those in the magnetotail. In parallel, recent results from the Grid Agnostic MHD for Extended Research Applications (GAMERA) global simulations (Zhang et al., 2021) also support a largely closed magnetosphere. However, there exists a crescent of open flux (with substantial variability on the rotation period) that surrounds the closed polar region (we avoid using the terminology "polar cap" to avoid confusion with the terrestrial open polar cap). Much of the closed polar flux maps to an extended region along the dawn flank.

The purpose of this manuscript is to the revisit the structure (and associated terminology) and dynamics of Jupiter's dawnside magnetosphere using the wealth of Juno data and insights from GAMERA simulations. We intend to offer clarity and context to specific historical terminology based on these recent advances in understanding. Specifically, we will investigate a 2-3 hour periodicity seen in the Juno magnetometer and thermal plasma data and attempt to relate these periodicities to possible azimuthal and radial density structure of the magnetodisc.

# 2 Methods

## 2.1 Juno Data

For this study data was provided by the Juno spacecraft's Magnetometer (MAG) (Connerney et al., 2017), Jovian Auroral Distribution Experiment (JADE) instrument (McComas et al., 2017), and wave (Waves) instrument (Kurth et al., 2017). The JADE instrument provides ion fluxes in the range of 0.01 to 50 keV/q. Density moments for Juno orbits 5 to 26 and for radial distances less than ~50 $R_J$ have been published by Huscher et al. (2021) and compare favorably with the trends in mean JADE counts (i.e., averaged over energy); thus, we use JADE mean counts as a proxy for density variations. The Waves instrument can infer electron density based on the electron plasma cutoff frequency. We use the Waves data together with the JADE mean counts to categorize regions of the magnetosphere based on qualitative characteristics of density variations. The trapped continuum radiation seen in the Waves data can be used to determine the electron density in cases of sufficient density. When density falls to very low values (e.g., $< 10^{-3}$ cc), the continuum radiation cutoff frequency falls below lowest frequency ($<$ 100 Hz), making large density variations easy to identify with sharp contrast in the continuum radiation. All data was taken from within the magnetosphere using the magnetopause boundary crossings defined by Ma et al. (2022).

## 2.2 Periodic Wave Power Analysis

A key diagnostic of structure (and dynamics) is periodic behavior of the magnetodisc. A step by step analysis was done to understand periodicities on the scale of 1-10 hours produced by magnetic field and density fluctuations. These steps are outlined in Figure 1. For the magnetic field, we focus on periodic fluctuations in the perpendicular component, serving as a proxy for possible Alfvénic activity (e.g., related to flow shear and/or transport processes) though compressional modes may also be present. To detect these transverse fluctuations the magnetometer data was rotated into a mean-field-aligned (MFA) coordinate system (Khurana & Kivelson, 1989). A 24-minute boxcar average on the magnetometer data provided a background magnetic field. Rotation into the MFA coordinate system provides the data in terms of fluctuations perpendicular and parallel to the average background field direction. For density, we use mean JADE counts as a proxy for density fluctuations. Typically, wave magnetic field amplitude is largest in regions of high density because the corresponding wave speed is small, so we expect the largest wave power to be found in the equatorial regions.

For periodic analysis the Continuous Wavelet Transform (CWT) was used, a technique for analyzing a time-dependent signal for periodic behavior (Torrence & Compo, 1998). This is particularly important for the non-stationary signals generated by Juno's motion through the plasmadisc. The wavelet transform is

$$W_i(t,\tau)=\sum_{i=0}^{N-1}\frac{\delta B_\perp}{\sqrt{\tau}}\psi^*\left[\frac{t_j-t}{\tau}\right]\Delta t \tag{1}$$

where $\psi(u) = \pi^{-1/4}e^{i\omega_0 u}e^{-u^2/2}$ is the base Morlet mother wavelet with characteristic frequency ($\omega_0$) of the underlying wave in the Gaussian-shaped wavelet packet. For this study we set $\omega_0 = 6$ (Farge, 1992). The wavelet is then scaled through different frequencies by varying packet width ($\tau$) and shifted along the signal. The CWT analysis yields a frequency-time spectrogram (hereafter referred to as the CWT). However, due to the nature of the CWT method, the maximum wavelet scale and therefore the smallest frequency able to be analyzed is dependent on the size of the input data signal. This introduces computational errors when the wavelet at larger scales can be cut off by the edges of the data window. These errors accumulate in the cone of influence, lining the outer portion of the CWT, effectively shrinking the usable data. To reduce the effects of the cone of influence and while still allowing for relatively small windows of data to be analyzed, data spanning no less than 2.5 days was used.

**Figure 1.** Periodic wave power analysis for a data window spanning the 1st-4th of March 2017. (Top-left) Total perpendicular fluctuation from the MFA magnetic field. (Bottom-left) Continuous Wavelet Transform of the perpendicular MFA component with the cone of influence removed. Analysis is limited to a frequency range corresponding to the periods of 1 hr and 10 hrs. (Right) Power Spectral Density of the CWT.

The Power Spectral Density (PSD) can be found from the CWT, and gives insight into periodic wave power. The PSD is simply an integration of the CWT across time, yielding the total wave power within the window as a function of frequency, or

$$PSD_i(\tau) = \frac{2}{N}\sum_{j=1}^{N}|W_i(t_j,\tau)|^2 \tag{2}$$

$N$ is the total steps, $|W_i(t_j,\tau)|^2$ being the total wave power from the CWT spectrum with a scale factor (inverse of frequency) of $\tau$, $i$ are the indices of the frequency domain, and $j$ are the indices across the time domain.

Wave power will increase with density, along with filtering of the data the PSD will become dominated by wave power from plasma interactions in higher density regions. The plasma sheet sweeps by the spacecraft every $\sim$10 hours and as shown in Figure 1 an expected peak at 10 hours appears in the PSD. However, due to Jupiter's $\sim\ 10^\circ$ dipole tilt, Juno can encounter the dense plasmasheet twice per rotation. While motion of the Juno spacecraft is sinusoidal in the $z_{cent}$ coordinate (Phipps & Bagenal, 2021), the density profile is exponential, resulting in a broadband power spectrum that can include harmonics of the 10-hour period. It should be noted that the harmonic signatures could be present in our time series analysis and periodicities in the 2-3 hour range could be associated with the $m = 3,4$ harmonics of the 10-hour period (where $m = 1$ refers to the fundamental, 10-hour period). Included in the electronic supplement are additional examples of our time series analysis showing the PSD with harmonics of the 10-hour period. We note the variability in 10 vs. 5 hour wave power as well as variable peaks in roughly the 2 to 3 hour range.

The identification of periodic activity is done by running a peak finding method on each PSD calculation to find peaks in wave power (Hereafter referred to as active periods). (The specific peak finding algorithm used was the Python "scipy.signal.find_peaks" method using the default parameters.) Active periods are counted and binned in a histogram to show in which periods we see substantial wave power.

## 2.3 Global simulations

The GAMERA model is an upgraded/modernized version of the multi-fluid Lyon-Fedder-Mobarry (MFLFM/GAMERA) global magnetosphere model which has been used extensively to study solar wind - magnetosphere interactions (Lyon et al., 2004; Zhang et al., 2019). The ideal magnetohydrodynamics (MHD) equations are solved with a finite volume (FV) numerical method. A major advantage of the MFLFM/GAMERA simulation is the combination of a high-order reconstruction scheme with an aggressive total variation diminishing (TVD) limiter that preserves steep gradients with little numerical dissipation or dispersion during advection. Minimizing numerical diffusion is crucial for resolving the magnetopause boundary (i.e, KH instability, Zhang et al. (2018)), internal transport processes, and the magnetic field topology of the high latitude polar region (Zhang et al., 2021). The FV techniques allow MFLFM/GAMERA to complete the calculation on a nonorthogonal, curvilinear grid adapted to the Jupiter magnetospheric problem, i.e. cells that are smaller across the nominal bow shock than parallel to it. The spherical grid extends 100 Jupiter radii ($R_J$) in the sunward direction, 1000 $R_J$ in the anti-sunward direction, and $\pm$300 $R_J$ in the directions perpendicular to the Sun-Jupiter axis. The grid resolution is non-uniform with 0.2 $R_J$ near the magnetopause and approximately 0.15 $R_J$

near the inner magnetosphere. The inner boundary of the simulation is at 6 $R_J$ (i.e., at the orbit of Io) in order to simplify the implementation of mass loading.

The simulation uses only a single fluid (protons) with a mass loading rate of 1000 kg/s, introduced in the equatorial region of the inner boundary. We note that this simplification is adequate for addressing periodicities in the magnetodisc, but would not be appropriate for direct comparison of, e.g., density. The mass loading module performs an extra step after the hydrodynamic update but before the Lorentz force and magnetic field updates (Varney et al., 2016). The extra mass fluxes, momentum fluxes, and energy fluxes through the inner interface are calculated from the mass loading parameters, and the active cells adjacent to the inner boundary interface are updated accordingly. This method ensures that the mass loading rate exactly equals the physical rate without creating numerical mass loading through the MHD solver.

As a single-fluid simulation, the inner "iogenic" source was the only source of protons besides the solar wind. Ionospheric outflow was not included, and absent solar wind variability, the simulation was subject to a considerable startup transient period, during which the high latitude regions were significantly modified. The combined (bulk) density profiles from a multi-fluid simulation, where solar wind and Io plasma are separate fluids, were qualitatively similar to the single-fluid results. The single-fluid simulation has the benefit of being computationally less expensive than the multi-fluid simulation. The main disadvantage was not being able to distinguish the exact source of the mass in the magnetotail, but we emphasize that these simulations were only being used to establish the plausibility of a highly structured magnetodisc.

The simulations were driven by idealized SW and interplanetary magnetic field (IMF) conditions ($V = 400$ km/s, $B_y = 0.5$ nT), consistent with the average solar wind dynamic pressure ($\sim$0.05 nPa) at Jupiter (Jackman & Arridge, 2011). For the purpose of this numerical experiment, the dipole tilt angle of Jupiter's magnetosphere was set to zero in order to remove hemispheric asymmetries and simplify the analysis. The magnetosphere-ionosphere coupling is adapted from the Magnetosphere Ionosphere Coupler/Solver (MIX) model for geospace with constant Pedersen conductance set to 0.5 mho and zero Hall conductance (Merkin & Lyon, 2010). We solve the ionospheric current closure in the rotating frame and therefore the electric field at the inner boundary includes both the corotation electric field and the electrostatic potential from current closure.

# 3 Results and Discussion

## 3.1 Identification of magnetospheric regions

As shown by Zhang et al. (2021) the dawnside magnetosphere is composed of a non-corotating closed polar flux region along the dawn/tail flank formed by flux pileup in a rapidly rotating magnetosphere, a corotating inner (closed) magnetodisc, and a transition region that potentially contains open flux, mapping, on average, to a crescent-shaped polar region. We note that the open flux was shown to be highly variable on the 10-hour rotation period, suggesting intermittent reconnection is operating in the simulations.

The overall magnetic structure of the dawn to midnight magnetosphere is consistent with that of a *magnetodisc*, i.e., dominated by the radial and azimuthal components of the magnetic field. While Delamere and Bagenal (2010) used the term "cushion" (i.e., dominated by the vertical magnetic field component, $B_\theta$) for the outer dawnside magnetosphere, we suggest abandoning this terminology given the absence of a cushion region as reported by Gershman et al. (2018). Instead, the governing property of our magnetosphere regions will be the vertical plasma distribution.

Juno's orbital precession is downward/southward. Due to this precession the dwell times near the equatorial region in the outer magnetosphere became small after orbit $\sim$15. As a result, all data was limited to the inbound portions of orbits 1-15. An analytical model of Jupiter's plasma sheet by (Phipps & Bagenal, 2021) was then used for verification of the spacecraft's proximity to the center of the plasma sheet, measured by a vertical distance $z_{cent}$. Using mean JADE counts as a proxy for plasma density as well as

**Figure 2.** Juno Magnetometer (Top), Mean JADE Counts (Middle), and Waves (Bottom) data from start to perijove of Orbit 7, showing the outer flux pileup region (grey), plasmadisc (red), and intermediate region (purple).

**Figure 3.** Orbital path of Juno for orbits 1-15. Shading when the spacecraft enters the pileup region, intermediate region between the pileup and disk, and the plasmadisc region.

the spacecraft's Waves instrument, windows of time were hand picked and categorized as: (a) a *dawn-side flux pileup* region (Zhang et al., 2021; Delamere & Bagenal, 2013), (b) an inner *plasmadisc* region, and (c) an *intermediate* region.

The *flux pileup* region was identified by relatively uniform density as a function of $z_{cent}$ (e.g., $<10\times$ variation in mean JADE counts), implying a large scale height. We argue that this region is similar to the "boundary layer" region identified by (Gurnett et al., 1980), noting that actual magnetopause boundary layer likely has a more limited radial spatial extent. The flux pileup region could also be similar to the tailward-flowing "magnetospheric wind" region described by Cheng and Krimigis (1989); therefore, we do not expect centrifugal plasma confinement in the flux pileup region due to non-corotational flows. In contrast, large 10-hour fluctuations in mean JADE counts (e.g., two to three orders of magnitude) and Waves data (e.g., continuum radiation $+<$ 100 Hz) as a function of $z_{cent}$ were considered properties of the *plasmadisc* region. Here the plasma is assumed to be strongly centrifugally confined with large corotational flows. The plasmadisc region could be similar to the inner plasmasphere of (Cheng & Krimigis, 1989). We also identified an *intermediate* region, exhibiting a seeming mix of these two limiting cases. The intermediate case could be similar to the plasma sheet region of (Cheng & Krimigis, 1989) and may be the transition to substantially subcorotational flow. It should also be noted that Zhang et al. (2021) showed that open flux can be found between the centrifugally-confined magnetodisc and the closed polar flux. The open flux is highly variable on the planet's rotation period and we suggest that the intermediate region may be capturing some the variable open flux (see Section 3.3). The open flux regions are likely associated with very low density, but we caution identifying these low-density regions as the *lobe* due to variability and stark difference with the terrestrial magnetic topology (e.g., see Zhang et al. (2021) Figure S6).

The identified regions for Orbit 7 are shown in Figure 2 using Juno magnetometer (top), JADE mean counts (middle), and Waves (bottom) data. We note the magnetosphere for this orbit was considered unperturbed as the aurora showed a continuous quiet morphology (Yao et al., 2019). The outer flux pileup region (grey), plasmadisc (red), and intermediate (purple) are shown. The flux pileup region (grey) shows little variation in JADE mean counts and Waves data cutoff frequency. The plasmadisc shows large amplitude fluctuations of uniform spacing as Juno traverses through the confined structure. The intermediate region shows smaller uniformly spaced fluctuations with some areas punctuated by larger non uniform fluctuations. We suggest that the intermediate region could be a transition between the pileup and plasmadisc regions and/or could be indicative of temporal variability (e.g., solar wind dynamic pressure). The remaining orbits are shown in the electronic supplement. Figure 3 summarizes the selected regions. A lack of intermediate regions identified within the first 6 orbits is apparent, this is due to the lack of plasma data as well as numerous magnetopause boundary crossings making accurate categorization rather difficult. We note that the transition from a plasmadisc-like configuration (red) to a flux pileup region (black) is roughly consistent with the Voyager 1 and 2 transition at $>$ 80 $R_J$ (Gurnett et al., 1980), though Juno observations indicate significant variability from one orbit to another. The transition from a plasmadisc to intermediate configuration (yellow) occurs between 60 and 80 $R_J$. We also note the peculiar feature of Orbit 12 where the innermost region is identified as intermediate case, contrary to expectation for a well-confined plasmadisc.

**Figure 4.** Histogram of the peaks in power spectral density in the JADE mean counts data split into the three regions. Flux pileup (Top), Intermediate (Middle), and the plasmadisc region (Bottom).

**Figure 5.** Histogram of the peaks in power spectral density in the magnetometer data split into the three regions. Flux pileup (Top), Intermediate (Middle), and the plasmadisc region (Bottom).

## 3.2 Periodicities in Juno MAG and JADE data

Figures 4 and 5 show the histogram of peaks in the PSD of JADE mean counts and magnetometer data, respectively. We note that peaks for periods less than five hours were identified by the peak finding method in roughly 65 of the 70 selected intervals, demonstrating the persistence of this characteristic. Both distributions are split into the three identified regions. The number of cases as a function of region is due to the increasing spacecraft dwell time in the outer magnetosphere. The peaks at 10 and 5 hours are clearly evident in all regions, while peaks are also found in the 2 to 3 hour range. The magnetic field data show a consistent peak near (but greater than) 3 hours in all three regions, while the JADE mean counts show consistent 3-hour peaks in the intermediate and plasmadisc regions. It should be noted that the ∼3-hour peak is roughly the $m = 3$ harmonic, but with low statistics and peaks occurring between the harmonics we suggest that this could also be indicative of physical density structure. Peaks occurring at shorter periods may be related to a turbulent spectrum that characterizes the magnetic field spectrum (Ng et al., 2022).

To evaluate the harmonic structure of the base 10-hour rotation period, a simple analytic model of Juno's sampling of the plasmadisc was created (i.e., Gaussian density profile as a function of $z_{cent}$, where $z_{cent}$ is sampled in sinusoidal manner similar to the Juno trajectory. See electronic supplement for details.). To mimic Juno data the model was tested for varying levels of plasma confinement similar to the separate identified regions, as well as varying the offset of the sinusoidal trajectory from the centrifugal equator plane. For large offsets we found the 10-hour period showed very strongly with the $m = 2$ and $m=3$ harmonics appearing. Varying the confinement slightly increased the prominence of the harmonics, however the harmonics still yielded less wave power than the base frequency. For no offset, the 5-hour period dominated ($m=2$) along with the $m=4$ harmonic. This simple model showed that we can expect to see the harmonics appear in the CWT analysis, but at varying degrees through the Juno orbit. We emphasize that harmonics will contribute to the PSD in the 2-4 hour range; however, with significant variability in amplitude, broadband wave power, and with peaks also occurring at intermediate values, we argue that a separate physical mechanism is likely responsible.

An additional mechanism for periodic behavior are resonant cavity eigenoscillations. For Saturn, Rusaitis et al. (2021) demonstrated that the magnetodisc resonant cavity can produce a 3-hour eigenoscillation. If the plasmadisc is highly structured in density, then a consistent eigenfrequency is unlikely, but the eigenmodes could instead span a broader range of frequencies. As we will show below (Section 3.3), GAMERA simulations support a highly structured plasmadisc that could contribute to the observed periodicities.

## 3.3 GAMERA simulations

The simulation achieved a steady-state configuration at roughly 200 hours when density structures transported from the inner magnetosphere take form and coalesce into an $m \sim 5$ to 10 azimuthal structure. The structured magnetodisc is bounded by extremely low density regions (e.g., $< 10^{-3}$ cm$^{-3}$), eventually reaching the density floor of $10^{-4}$ cm$^{-3}$ that is imposed to ensure numerical stability. In the latest stage of the simulations, the density variations grow in amplitude and likely result from an inadequate proton source

**Figure 6.** GAMERA simulation showing density variations in the equatorial plane.

**Figure 7.** GAMERA simulation showing density variations (left) and open vs. closed flux (right) in the meridional plane. The contour lines encompass regions of open field lines. The upper left image shows density in the equatorial plane with the red line denoting the location (LT = 3) of the meridional plane.

**Figure 8.** Juno Orbit 7 density variations from JADE moments (Huscher et al., 2021) for radial distances from 30 to 50 $R_J$ and $|z_{cent}| < 5$. The thick black line is the average profile for all crossings. The thick blue curve is the fitted Gaussian, showing a much broader distribution ($\sigma = 3$ $R_J$) as a function of $z_{cent}$.

**Figure 9.** Relative density variations from Juno/JADE (Huscher et al., 2021) for radial distances from 30 to 50 $R_J$ compared with variations from GAMERA simulations for radial distances from 10 to 60 $R_J$. For the respective Gaussian fits, $\sigma = 46.0$ and $\sigma = 41.4$.

for the high latitude regions. For comparison with the Juno/JADE observations, we have selected the interval between 200 and 350 hours because of the remarkable consistency with the data (described below).

Figure 6 shows the density structures at t = 291.4 hours. We find that the dawn/midnight sector is structured by both the radial transport of density "arms" from the inner magnetosphere as well as low density flux tubes (due to tail reconnection) injected sunward and adjacent to the dawnside magnetopause boundary. The confluence of outward transport and reconnection flows leads to substantial variability in this dawn flank region of the magnetosphere. Adding to further complexity is the preponderance of global-scale Kelvin-Helmholtz waves at the magnetopause boundary.

Figure 7 shows density (left) and open vs. closed flux (right) in the meridional plane with contours encompassing regions of open flux taken at roughly 3 LT (similar to Juno Orbit $\sim$ 12). Here we see substantial variations in density with latitude (or $z_{cent}$). In the inner magnetosphere, the magnetodisc is bounded by low-density regions (e.g., $10^{-3}$ $cm^{-3}$). The outer magnetosphere, on the other hand, exhibits a much larger scale-height with less contrast in density as a function of $z_{cent}$, consistent with the findings of Gurnett et al. (1980). The open flux regions are highly variable during the planetary rotation period. At this particular time, it is evident that extremely low density (e.g., $< \ 10^{-3}$ $cm^{-3}$) can be found on closed field lines; therefore, the simulations suggest that density is not a reliable measure of field topology. In fact, there are instances where the density is higher on open field lines compared with the density on closed field lines at smaller $|z_{cent}|$. The polar closed flux (flux pileup region) shows consistently low density at high latitude.

## 3.4 GAMERA vs. JADE relative density variations

The empirical scale height of Jupiter's magnetodisc was given by (Bagenal & Delamere, 2011), as a monotonically increasing function with an asymptotic value of roughly 4 $R_J$. However, Huscher et al. (2021) showed that for a given plasma sheet crossing, the density $e$-fold was typically much less than 4 $R_J$ with considerable variability. Figure 8 illustrates this property for orbit 7 between 30 and 50 $R_J$ and for $|z_{cent} < 5|$, where $z_{cent}$ is the vertical distance from the centrifugal equator plane as defined by Phipps and Bagenal (2021). The density values are a 40-point rolling mean of the moments from Huscher et al. (2021) (with relative uncertainty <1000%), with color indicating time to separate the various crossings. The black line is a binned average and the blue line is a Gaussian fit to the binned average with a scale height of 2.6 $R_J$. The variations in peak density and $1/e$

**Figure 10.** Histogram of GAMERA density PSD peaks.

**Figure 11.** Histogram of GAMERA magnetic field PSD peaks.

change in density functions of $z_{cent}$ are clearly evident, consistent the with conclusions of Huscher et al. (2021) that the plasma sheet shows considerable small-scale structure.

To further quantify the variability of the plasma sheet, we have compared the relative variations in peak density between consecutive crossings. We applied a peak-finding algorithm to identify density maxima for Juno Orbits 5 to 26. Because of the Juno orbital precession, we admitted time intervals between maxima ranging from 2 to 11 hours. In the early orbits, many of consecutive crossings occurred $<$ 10 hours. Figure 9 is a histogram of the relative variations in log density. The fitted Gaussian (i.e., $\exp(-(x - x_0)^2/\sigma^2)$) has $\sigma = 46.0$. The bias toward negative density variations is due to the general trend of decreasing density with radial distance. Figure 9 also shows the relative density variations in the GAMERA simulation. To mimic the Juno observations, we sampled the equatorial density in the dawn/midnight region at 10-60 $\mathrm{R_J}$ using an ensemble of sampling intervals ranging between 2 and 10 hours (i.e., 2, 4, 6, 8, and 10 hours). The width of the fitted Gaussian is $\sigma = 41.4$, remarkably consistent with the observations.

## 3.5 Periodicities in the GAMERA simulations

For this study 44 static points lying in the dawn-side equatorial plane were selected. To conduct this analysis in a similar fashion as the Juno data we split the points into two regions: an inner region ($10\ \mathrm{R_J} < R < 60\ \mathrm{R_J}$) bounding an area that housed the density "arm" structure, and an outer region ($R > 60\ \mathrm{R_J}$) that contains a relatively uniform density distribution with intermittent low density flux tube injections from tail reconnection. We do not attempt to identify an intermediate region in the GAMERA simulations as $R \sim 60\ R_J$ qualitatively defines a distinct transition region. Again, the simulations were performed with steady solar wind conditions; thus, the magnetosphere is not subject to expansion and compression. Similar CWT analysis was done on each of the 44 points to get a distribution of peaks in the PSD (hereafter referred to as the active periods) for both the density and magnetic field fluctuations. The active periods for density fluctuations are shown in Figure 10 and active periods from magnetic field fluctuations are shown in Figure 11.

The active period distributions in both data sets exhibit a strong 10-hour period similar to the Juno data, attributed to the rotation period of the planet. The active periods in the density data (Figure 10) show a slight local maximum around 3-hours for $R < 60\ \mathrm{R_J}$, and a sharp peak between 2-3 hours with a steady increase in wave power as period decreases further for $R > 60\ \mathrm{R_J}$, which we attribute to a power law PSD with local maxima at shorter periods that the peak-finding algorithm identified but that we consider to be insignificant. The active period distribution for the magnetic field (Figure 11) shows a similar slight maximum at 3-hours for $R < 60\ \mathrm{R_J}$, with a decrease in wave power for $R > 60\ \mathrm{R_J}$. We expect a corotating $m = 3$ to 5 density structure to contribute in the 2-3 hour range at $R = 60\ \mathrm{R_J}$ (i.e., where $m$ is the number of density maxima on the azimuthal spatial domain), though subcorotation would support higher $m$ structures, consistent with Figure 6.

# 4 Conclusions

Using Juno data (JADE, MAG, and Waves) we have demonstrated that Jupiter's dawnside magnetosphere exhibits tremendous variability. Understanding the temporal vs. spatial aspects of this variability is an ongoing challenge. However, the overall meridional spatial structure is consistent with an inner, centrifugally-bound plasmadisc bounded by very low density regions and an outer region characterized by weak density variation in the vertical direction. Comparing with global GAMERA simulations, we have associated these regions with the simulated magnetic field topology. The outer magnetosphere contains closed flux, mapping to the high latitude polar region. Zhang et al. (2021) referred to this region as the *flux pileup region*. The low-density regions separating the inner and outer magnetosphere may contain open flux (Zhang et al., 2021).

While the gross meridional structural may be an adequate average representation, variability is clearly apparent from one orbit to another. Our qualitative assessment of three regions (i.e., outer flux pileup, inner plasmadisc, and intermediate transition) shows, very roughly, that the transition from a well-defined plasmadisc structure to the flux pileup region occurs between 60 and 100 $R_J$, and that the periodicities are present in all regions. This variability is likely to be a function of solar wind dynamic pressure and the expanded/compressed state of the magnetosphere. The intermediate cases could be associated with transitions between expanded/compressed configurations. Alternatively, the intermediate cases could be strongly influenced magnetotail dynamics under steady solar wind driving. Future simulations that include solar wind variability would be necessary to address the intermediate cases. Additionally, the state of the magnetosphere should be compared with Hubble Space Telescope observations of Jupiter's aurora to determine possible states of the system (Grodent et al., 2018; Yao et al., 2022).

The GAMERA simulations showed that the plasmadisc is highly structured, exhibiting radial density "arms". Other global simulations have shown similar structure (e.g., Tanaka et al. (2021)). The agreement between relative JADE density variations and the GAMERA density structures support the existence of such a highly structured plasmadisc and related magnetospheric dynamics. These structures could also account for the ~three-hour periodicity seen in the Juno data. A three-hour period is consistent with a corotating $m \sim 3$ structure or higher $m$ structures for subcorotational flows. Solar wind modulation from a Kelvin-Helmholtz-active magnetopause boundary could also contribute to the three-hour periodicity, where the solar wind advection time past the magnetospheric cavity is on the order of hours. Magnetotail dynamics could impose a periodicity, as periodic injection flows are seen in the GAMERA simulations, but we note that the injection flows are confined to the outer magnetosphere on the dawn flank. Finally, resonant cavity eigenmodes of the magnetodisc structure could be another alternative for the three-hour periodicity. We find the latter less likely due to the extremely different plasma conditions (and corresponding wave velocities) found throughout the dawnside magnetosphere.

Future investigations will include a comparison of plasma properties from the JADE and JEDI instruments with the GAMERA simulations. Additional simulations studies should include a multi-species treatment of the iogenic plasma, solar wind variations, sensitivity to ionospheric boundary conditions, ionospheric outflow, sensitivity to grid resolution, inclusion of a plasma heat source to account for the superthermal ion population. Test particle simulations should be conducted to assess the impact of drift physics on the periodicities, particularly in the injection flow regions. We also intend to employ information theory to understand possible nonlinear and causal relations in the simulations (Wing & Johnson, 2019). Collectively, these future studies could provide insights into periodicities on the ~hours time scale.

# 5 Data availability statement

The Waves data can be downloaded from Kurth and Piker (2022). We acknowledge useful discussions with Bill Kurth on the Waves data. JADE data can be download from Allegrini et al. (2022). The JADE density moments are available from Huscher et al. (2021). We acknowledge useful discussions with Rob Wilson on the JADE data. MAG data can be accessed from Connerney (2022). The figure data used in the paper are available in Delamere and Schok (2023).

# References


Allegrini, F., Wilson, R. J., Ebert, R. W., & Loeffler, C. (2022). *JUNO JADE CALIBRATED SCIENCE DATA, NASA Planetary Data System, [Dataset].* Retrieved from https://doi.org/10.17189/1519715

Bagenal, F., & Delamere, P. A. (2011, May). Flow of mass and energy in the magnetospheres of Jupiter and Saturn. *Journal of Geophysical Research (Space Physics)*, *116*(A5), A05209. doi: 10.1029/2010JA016294

Cheng, A. F., & Krimigis, S. M. (1989, September). A model of global convection in Jupiter's magnetosphere. *J. Geophys. Res.*, *94*, 12003-12008. doi: 10.1029/JA094iA09p12003

Connerney, J. E. P. (2022). *Juno MAG CALIBRATED DATA J V1.0, JNO-J-3-FGM-CAL-V1.0, NASA Planetary Data System, [Dataset].* Retrieved from https://doi.org/10.17189/1519711

Connerney, J. E. P., Benn, M., Bjarno, J. B., Denver, T., Espley, J., Jorgensen, J. L., ... Smith, E. J. (2017, Nov 01). The juno magnetic field investigation. *Space Science Reviews*, *213*(1), 39–138. Retrieved from https://doi.org/10.1007/s11214-017-0334-z doi: 10.1007/s11214-017-0334-z

Delamere, P. A., & Bagenal, F. (2010, October). Solar wind interaction with Jupiter's magnetosphere. *Journal of Geophysical Research (Space Physics)*, *115*, 10201-+. doi: 10.1029/2010JA015347

Delamere, P. A., & Bagenal, F. (2013, November). Magnetotail structure of the giant magnetospheres: Implications of the viscous interaction with the solar wind. *Journal of Geophysical Research (Space Physics)*, *118*(11), 7045-7053. doi: 10.1002/2013JA019179

Delamere, P. A., Otto, A., Ma, X., Bagenal, F., & Wilson, R. J. (2015, June). Magnetic flux circulation in the rotationally driven giant magnetospheres. *Journal of Geophysical Research (Space Physics)*, *120*, 4229-4245. doi: 10.1002/2015JA021036

Delamere, P. A., & Schok, A. (2023). *Periodicities and plasma density structure of Jupiter's dawnside magnetosphere, figshare, [figure].* Retrieved from https://doi.org/10.6084/m9.figshare.21934427.v1

Farge, M. (1992). Wavelet transforms and their applications to turbulence. *Annual Review of Fluid Mechanics*, *24*(1), 395-458. Retrieved from https://doi.org/10.1146/annurev.fl.24.010192.002143 doi: 10.1146/annurev.fl.24.010192.002143

Gershman, D. J., DiBraccio, G. A., Connerney, J. E. P., Bagenal, F., Kurth, W. S., Hospodarsky, G. B., ... Bolton, S. J. (2018). Juno constraints on the formation of jupiter's magnetospheric cushion region. *Geophysical Research Letters*, *45*(18), 9427-9434. Retrieved from https://agupubs.onlinelibrary.wiley.com/doi/abs/10.1029/2018GL079118 doi: https://doi.org/10.1029/2018GL079118

Grodent, D. (2014, May). A Brief Review of Ultraviolet Auroral Emissions on Giant Planets. *Space Science Reviews*. doi: 10.1007/s11214-014-0052-8

Grodent, D., Bonfond, B., Yao, Z., Gérard, J.-C., Radioti, A., Dumont, M., ... Valek, P. (2018). Jupiter's aurora observed with hst during juno orbits 3 to 7. *Journal of Geophysical Research: Space Physics*, *123*(5), 3299-3319. Retrieved from https://agupubs.onlinelibrary.wiley.com/doi/abs/10.1002/2017JA025046 doi: https://doi.org/10.1002/2017JA025046

Gurnett, D. A., Kurth, W. S., & Scarf, F. L. (1980, January). The structure of the Jovian magnetotail from plasma wave observations. *Geophys. Res. Lett.*, *7*, 53-56. doi: 10.1029/GL007i001p00053

Huscher, E., Bagenal, F., Wilson, R. J., Allegrini, F., Ebert, R. W., Valek, P. W., ... Levin, S. M. (2021, August). Survey of Juno Observations in Jupiter's Plasma Disk: Density. *Journal of Geophysical Research (Space Physics)*,

*126*(8), e29446. doi: 10.1029/2021JA029446
Jackman, C. M., & Arridge, C. S. (2011, December). Solar Cycle Effects on the Dynamics of Jupiter's and Saturn's Magnetospheres. *Solar Phys.*, *274*, 481-502. doi: 10.1007/s11207-011-9748-z
Kennel, C. F., & Coroniti, F. V. (1977, June). Possible origins of time variability in Jupiter's outer magnetosphere. 2. Variations in solar wind magnetic field. *Geophys. Res. Lett.*, *4*, 215-218. doi: 10.1029/GL004i006p00215
Khurana, K. K., & Kivelson, M. G. (1989). Ultralow frequency mhd waves in jupiter's middlemagnetosphe. *Journal of Geophysical Research*, *94*(A5), 5241-5254.
Khurana, K. K., Kivelson, M. G., Vasyliunas, V. M., Krupp, N., Woch, J., Lagg, A., ... Kurth, W. S. (2004). Jupiter, the planet, satellites and magnetosphere. In F. Bagenal, T. E. Dowling, & W. B. McKinnon (Eds.), *Jupiter. the planet, satellites and magnetosphere* (p. 593-616). Cambridge Planetary Science.
Khurana, K. K., & Tsyganenko, N. A. (2002, December). A Global Model of Jupiter's Magnetospheric Field. *AGU Fall Meeting Abstracts*, A520+.
Kivelson, M. G., & Southwood, D. J. (2005, December). Dynamical consequences of two modes of centrifugal instability in Jupiter's outer magnetosphere. *Journal of Geophysical Research (Space Physics)*, *110*, 12209-+. doi: 10.1029/2005JA011176
Krimigis, S. M., Bostrom, C. O., Keath, E. P., Zwickl, R. D., Carbary, J. F., Armstrong, T. P., ... Lanzerotti, L. J. (1979, November). Hot plasma environment at Jupiter - Voyager 2 results. *Science*, *206*, 977-984. doi: 10.1126/science.206.4421.977
Kurth, W. S., Hospodarsky, G. B., Kirchner, D. L., Mokrzycki, B. T., Averkamp, T. F., Robison, W. T., ... Zarka, P. (2017, Nov 01). The juno waves investigation. *Space Science Reviews*, *213*(1), 347–392. Retrieved from `https://doi.org/10.1007/s11214-017-0396-y` doi: 10.1007/s11214-017-0396-y
Kurth, W. S., & Piker, C. W. (2022). *JUNO WAVES SURVEY STANDARD SCIENCE PRODUCTS, NASA Planetary Data System, [Dataset].* Retrieved from `https://doi.org/10.17189/1520498`
Lyon, J. G., Fedder, J. A., & Mobarry, C. M. (2004, October). The Lyon-Fedder-Mobarry (LFM) global MHD magnetospheric simulation code. *Journal of Atmospheric and Solar-Terrestrial Physics*, *66*, 1333-1350. doi: 10.1016/j.jastp.2004.03.020
Ma, X., Delamere, P. A., Schok, A., Wing, S., Johnson, J. R., & Liou, Y.-L. (2022). Jupiter's sheared flow unstable magnetopause boundary observed by Juno. *Journal of Geophysical Research.*
McComas, D. J., Alexander, N., Allegrini, F., Bagenal, F., Beebe, C., Clark, G., ... White, D. (2017, Nov 01). The Jovian Auroral Distributions Experiment (JADE) on the Juno Mission to Jupiter. *Space Science Reviews*, *213*(1), 547–643. Retrieved from `https://doi.org/10.1007/s11214-013-9990-9` doi: 10.1007/s11214-013-9990-9
McComas, D. J., & Bagenal, F. (2007, October). Jupiter: A fundamentally different magnetospheric interaction with the solar wind. *Geophys. Res. Lett.*, *34*, 20106-+. doi: 10.1029/2007GL031078
McComas, D. J., & Bagenal, F. (2008, May). Reply to comment by S. W. H. Cowley et al. on "Jupiter: A fundamentally different magnetospheric interaction with the solar wind". *Geophys. Res. Lett.*, *35*, 10103-+. doi: 10.1029/2008GL034351
Merkin, V. G., & Lyon, J. G. (2010, October). Effects of the low-latitude ionospheric boundary condition on the global magnetosphere. *Journal of Geophysical Research (Space Physics)*, *115*, A10202. doi: 10.1029/2010JA015461
Ng, C. S., Neupane, B. R., Delamere, P. A., & Damiano, P. A. (2022, January). A Turbulent Heating Model Combining Diffusion and Advection Effects

for Giant Planet Magnetospheres. *Geophys. Res. Lett.*, *49*(2), e96662. doi: 10.1029/2021GL096662

Phipps, P., & Bagenal, F. (2021). Centrifugal equator in jupiter's plasma sheet. *Journal of Geophysical Research: Space Physics*, *126*(1), e2020JA028713. Retrieved from `https://agupubs.onlinelibrary.wiley.com/doi/abs/10.1029/2020JA028713` (e2020JA028713 2020JA028713) doi: https://doi.org/10.1029/2020JA028713

Rusaitis, L., Khurana, K. K., Kivelson, M. G., & Walker, R. J. (2021, April). Quasiperiodic 1 Hour Alfvén Wave Resonances in Saturn's Magnetosphere: Theory for a Realistic Plasma/Field Model. *Geophys. Res. Lett.*, *48*(7), e90967. doi: 10.1029/2020GL090967

Staniland, N. R., Dougherty, M. K., Masters, A., & Achilleos, N. (2021, March). The Cushion Region and Dayside Magnetodisc Structure at Saturn. *Geophys. Res. Lett.*, *48*(6), e91796. doi: 10.1029/2020GL091796

Szalay, J. R., Clark, G., Livadiotis, G., McComas, D. J., Mitchell, D. G., Rankin, J. S., ... Bolton, S. J. (2022, May). Closed Fluxtubes and Dispersive Proton Conics at Jupiter's Polar Cap. *Geophys. Res. Lett.*, *49*(9), e98741. doi: 10.1029/2022GL098741

Tanaka, T., Ebihara, Y., Watanabe, M., Fujita, S., & Kataoka, R. (2021). Global simulation of the jovian magnetosphere: Transitional structure from the io plasma disk to the plasma sheet. *Journal of Geophysical Research: Space Physics*, *126*(6), e2021JA029232. Retrieved from `https://agupubs.onlinelibrary.wiley.com/doi/abs/10.1029/2021JA029232` (e2021JA029232 2021JA029232) doi: https://doi.org/10.1029/2021JA029232

Torrence, C., & Compo, G. P. (1998). A practical guide to wavelet analysis. *Bulletin of the American Meteorological Society*, *79*(1), 61-78.

Varney, R. H., Wiltberger, M., Zhang, B., Lotko, W., & Lyon, J. (2016, October). Influence of ion outflow in coupled geospace simulations: 1. Physics-based ion outflow model development and sensitivity study. *Journal of Geophysical Research (Space Physics)*, *121*, 9671-9687. doi: 10.1002/2016JA022777

Vasyliunas, V. M. (1983). Physics of the jovian magnetosphere. In A. J. Dessler (Ed.), (p. 395-453). Cambridge Planetary Science Series.

Wing, S., & Johnson, J. R. (2019). Applications of Information Theory in Solar and Space Physics. *Entropy*, *21(2):140*, https://doi.org/10.3390/e21020140.

Yao, Z. H., Bonfond, B., Grodent, D., Chané, E., Dunn, W. R., Kurth, W. S., ... Bolton, S. J. (2022). On the relation between auroral morphologies and compression conditions of jupiter's magnetopause: Observations from juno and the hubble space telescope. *Journal of Geophysical Research: Space Physics*, *n/a*(n/a), e2021JA029894. Retrieved from `https://agupubs.onlinelibrary.wiley.com/doi/abs/10.1029/2021JA029894` (e2021JA029894 2021JA029894) doi: https://doi.org/10.1029/2021JA029894

Yao, Z. H., Grodent, D., Kurth, W. S., Clark, G., Mauk, B. H., Kimura, T., ... Levin, S. M. (2019, November). On the Relation Between Jovian Aurorae and the Loading/Unloading of the Magnetic Flux: Simultaneous Measurements From Juno, Hubble Space Telescope, and Hisaki. *Geophys. Res. Lett.*, *46*(21), 11,632-11,641. doi: 10.1029/2019GL084201

Zhang, B., Delamere, P. A., Ma, X., Burkholder, B., Wiltberger, M., Lyon, J. G., ... Sorathia, K. A. (2018, January). Asymmetric Kelvin-Helmholtz Instability at Jupiter's Magnetopause Boundary: Implications for Corotation-Dominated Systems. *Geophys. Res. Lett.*, *45*, 56-63. doi: 10.1002/2017GL076315

Zhang, B., Delamere, P. A., Yao, Z., Bonfond, B., Lin, D., Sorathia, K. A., ... Lyon, J. G. (2021, April). How Jupiter's unusual magnetospheric topology structures its aurora. *Science Advances*, *7*(15), eabd1204. doi: 10.1126/sciadv.abd1204

Zhang, B., Sorathia, K. A., Lyon, J. G., Merkin, V. G., Garretson, J. S., & Wiltberger, M. (2019, sep). GAMERA: A three-dimensional finite-volume MHD solver for non-orthogonal curvilinear geometries. *The Astrophysical Journal Supplement Series*, *244*(1), 20. Retrieved from `https://doi.org/10.3847/1538-4365/ab3a4c` doi: 10.3847/1538-4365/ab3a4c

**Acknowledgments**

This paper is supported by NASA grants 80NSSC19K0822 and 80NSSC20K1279.

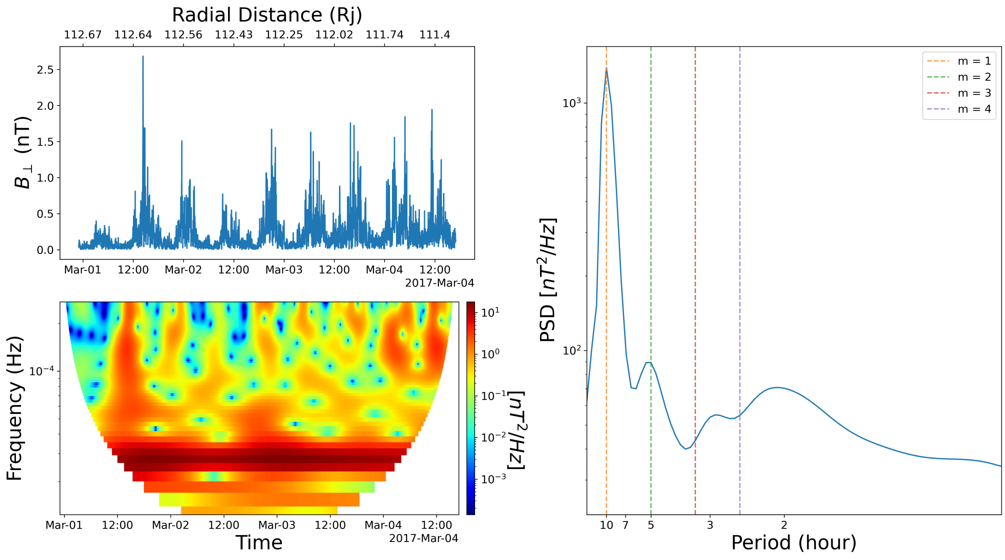
Radial Distance (Rj)
112.67 112.64 112.56 112.43 112.25 112.02 111.74 111.4
$B_\perp$ (nT)
2.5
2.0
1.5
1.0
0.5
0.0
Mar-01 12:00 Mar-02 12:00 Mar-03 12:00 Mar-04 12:00
2017-Mar-04
Frequency (Hz)
$10^{-4}$
$10^{1}$
$10^{0}$
$10^{-1}$
$10^{-2}$
$10^{-3}$
$[nT^2/Hz]$
Time
PSD $[nT^2/Hz]$
$10^{3}$
$10^{2}$
m = 1
m = 2
m = 3
m = 4
10 7 5 3 2
Period (hour)

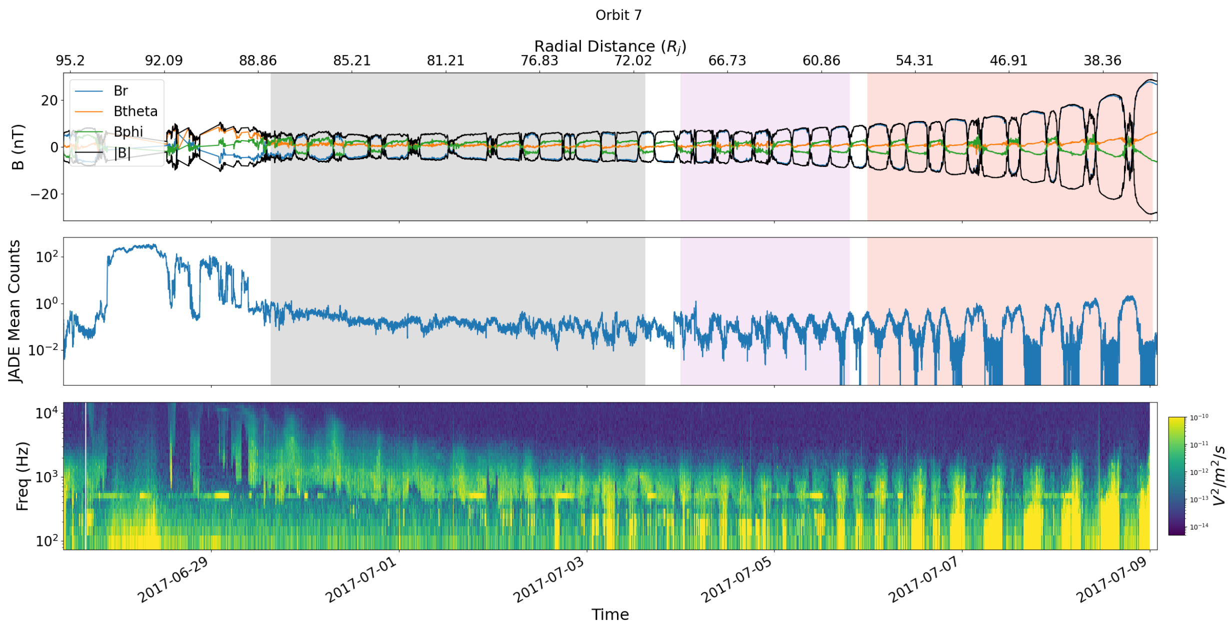
Orbit 7
Radial Distance ($R_j$)
95.2
92.09
88.86
85.21
81.21
76.83
72.02
66.73
60.86
54.31
46.91
38.36
Br
Btheta
Bphi
|B|
B (nT)
JADE Mean Counts
Freq (Hz)
$V^2/m^2/s$
2017-06-29
2017-07-01
2017-07-03
2017-07-05
2017-07-07
2017-07-09
Time

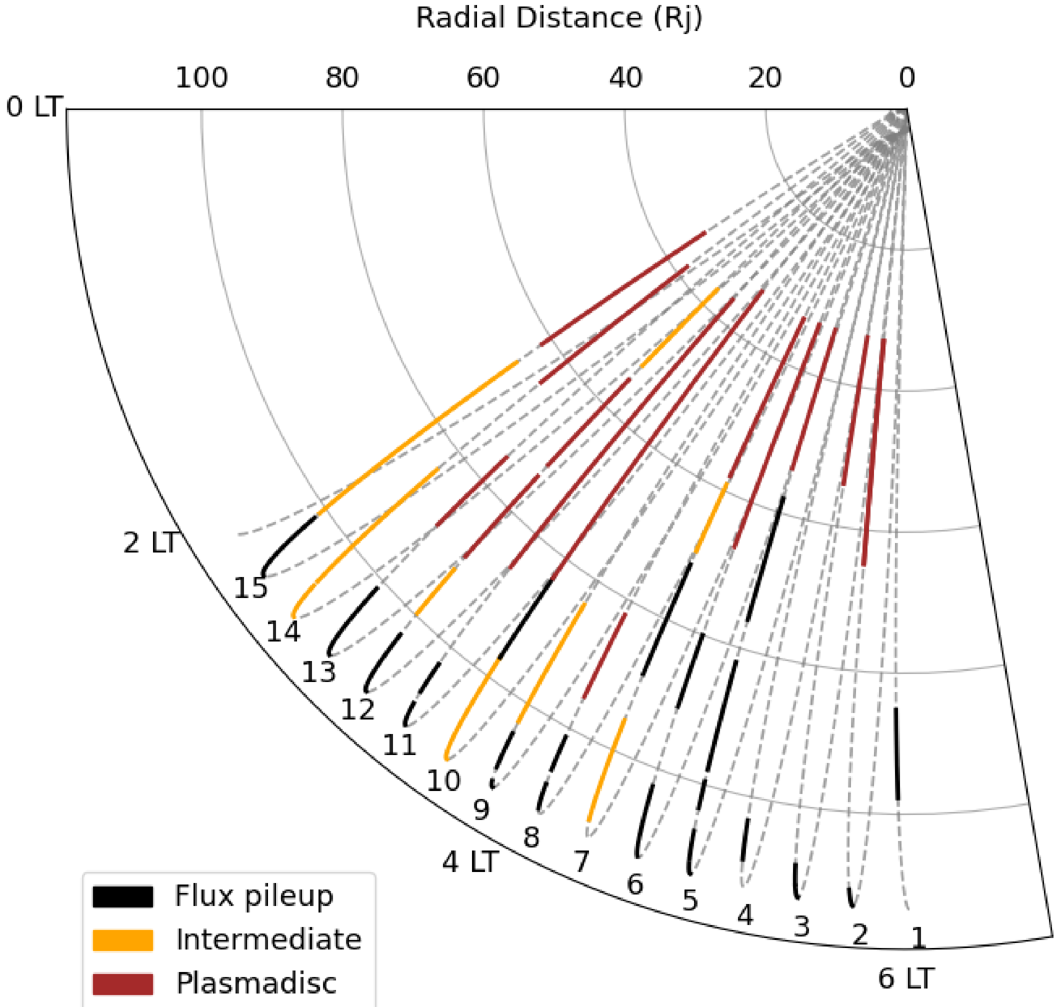

Radial Distance (Rj)
100
80
60
40
20
0
0 LT
2 LT
4 LT
6 LT
15
14
13
12
11
10
9
8
7
6
5
4
3
2
1
Flux pileup
Intermediate
Plasmadisc

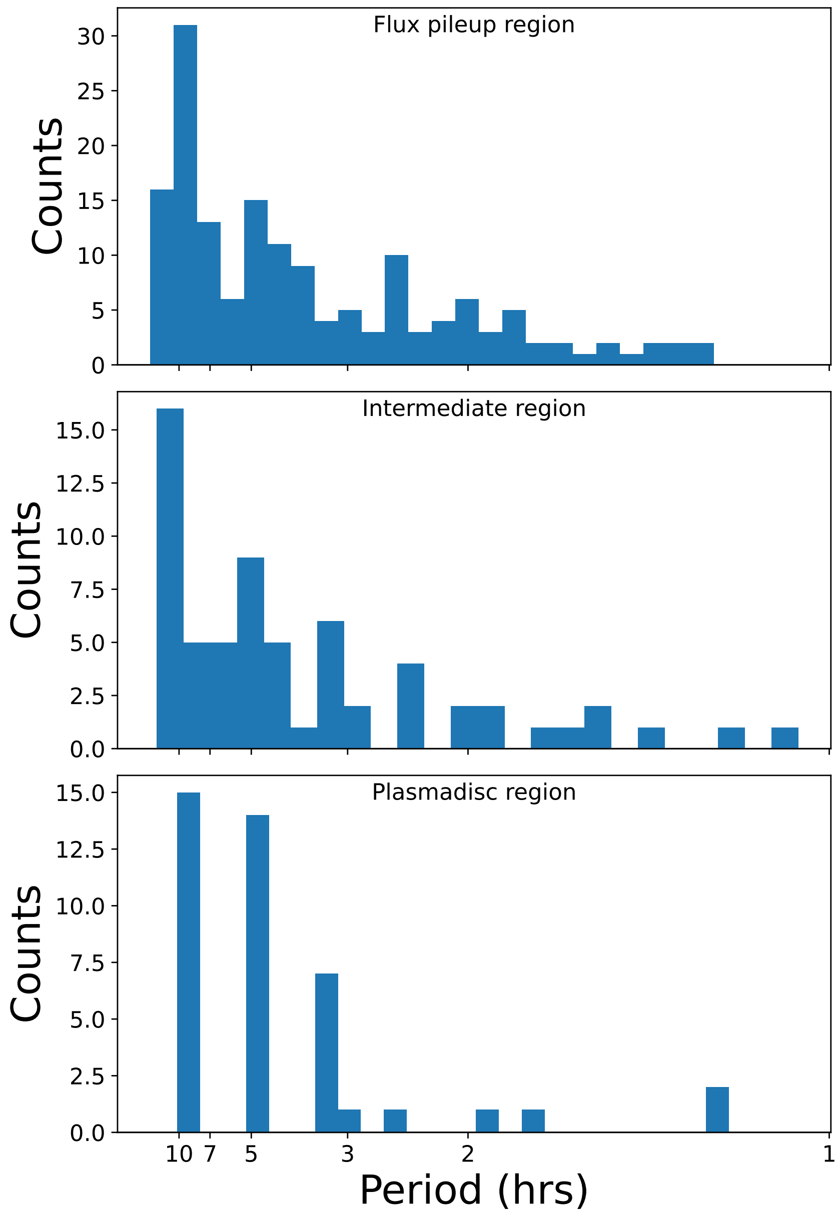

Flux pileup region
Counts
Intermediate region
Counts
Plasmadisc region
Counts
Period (hrs)

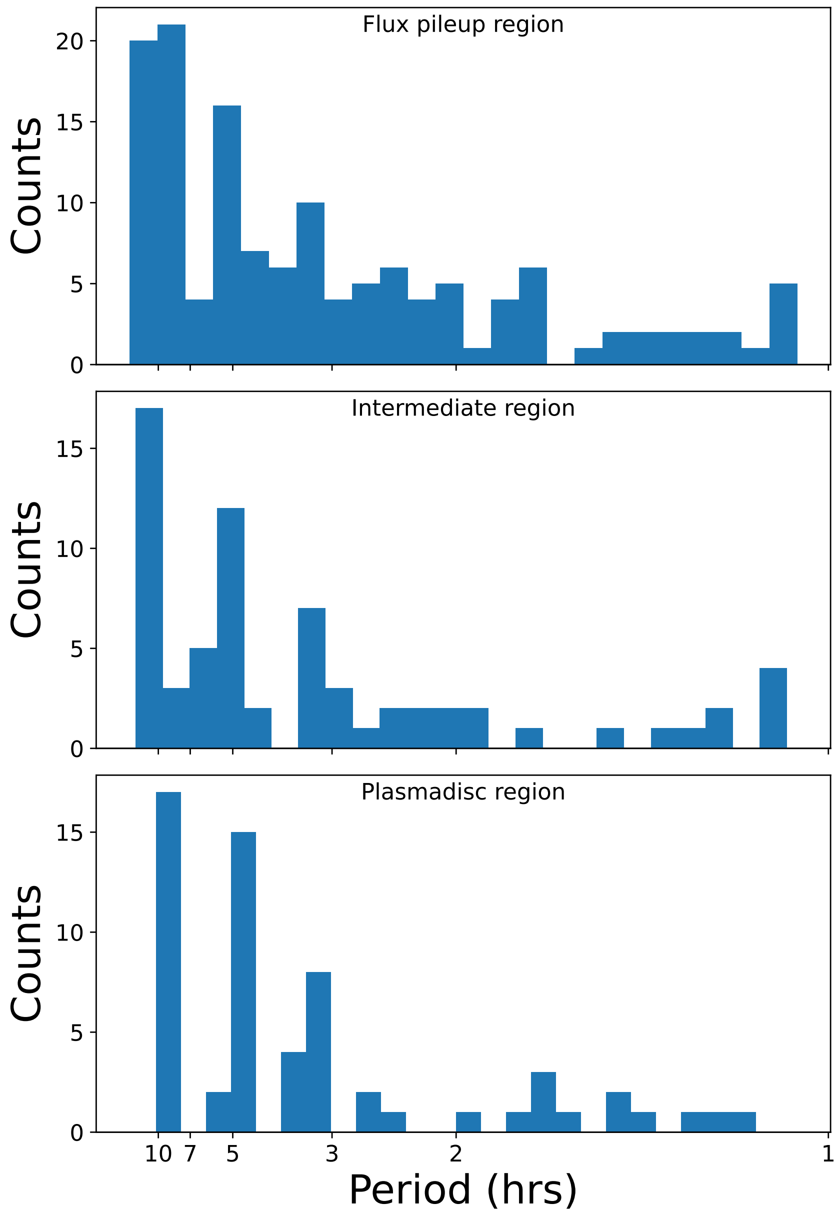
Flux pileup region
Counts
Intermediate region
Counts
Plasmadisc region
Counts
10 7 5 3 2 1
Period (hrs)

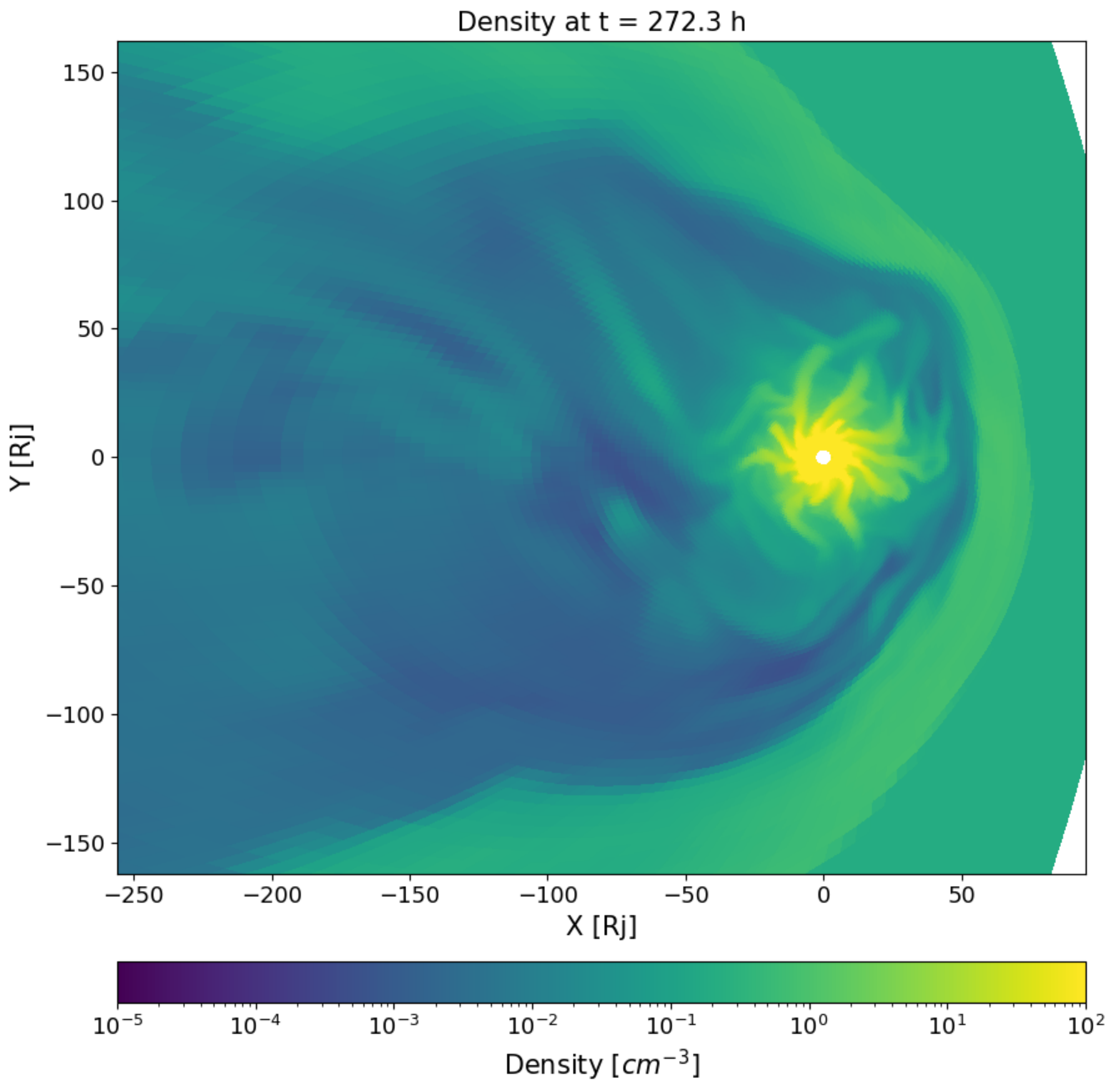
Density at t = 272.3 h
Y [Rj]
X [Rj]
150
100
50
0
−50
−100
−150
−250
−200
−150
−100
−50
0
50
$10^{-5}$
$10^{-4}$
$10^{-3}$
$10^{-2}$
$10^{-1}$
$10^{0}$
$10^{1}$
$10^{2}$
Density [$cm^{-3}$]

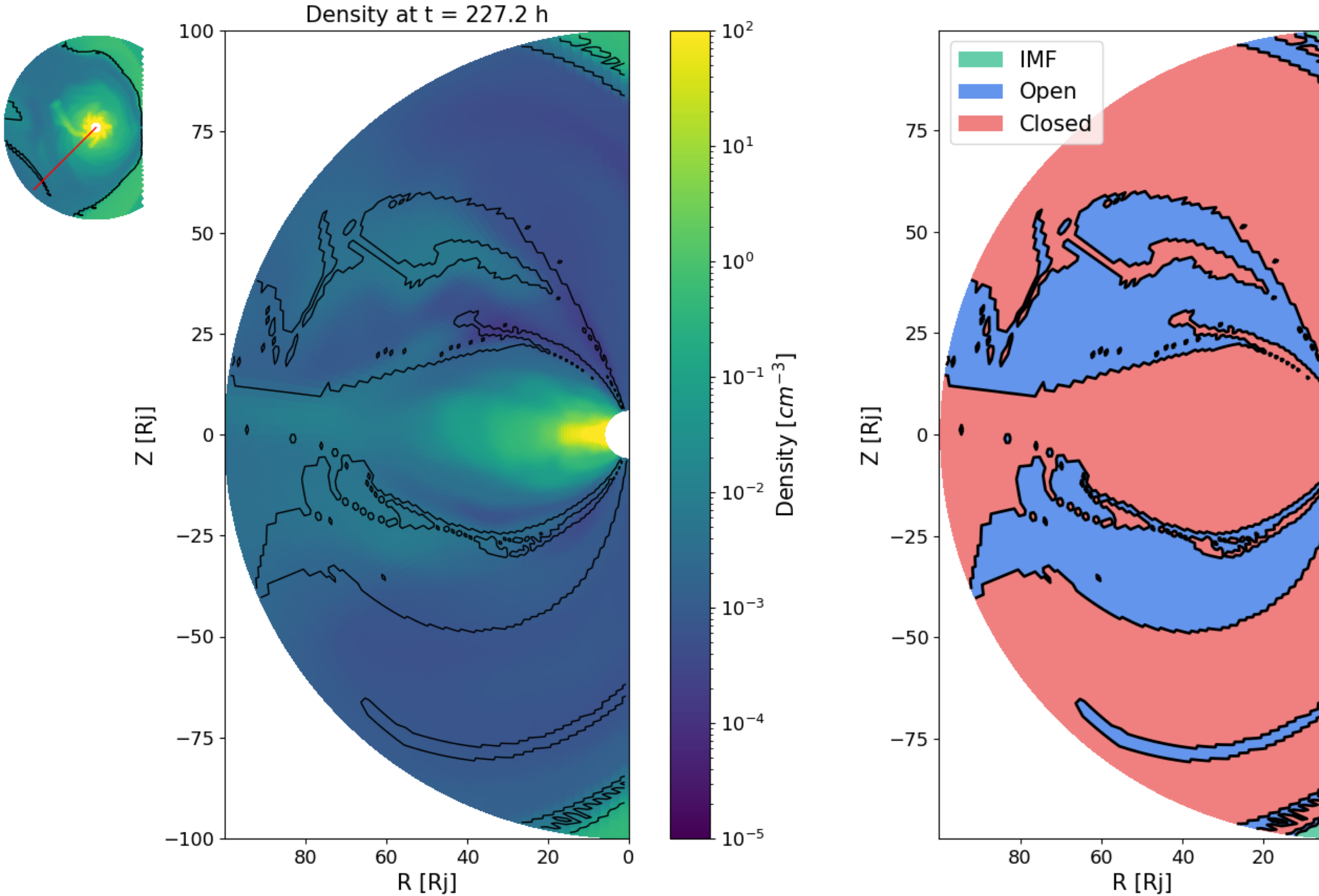

Density at t = 227.2 h
Z [Rj]
R [Rj]
Density [$cm^{-3}$]
100
75
50
25
0
−25
−50
−75
−100
80
60
40
20
0
$10^{2}$
$10^{1}$
$10^{0}$
$10^{-1}$
$10^{-2}$
$10^{-3}$
$10^{-4}$
$10^{-5}$
IMF
Open
Closed

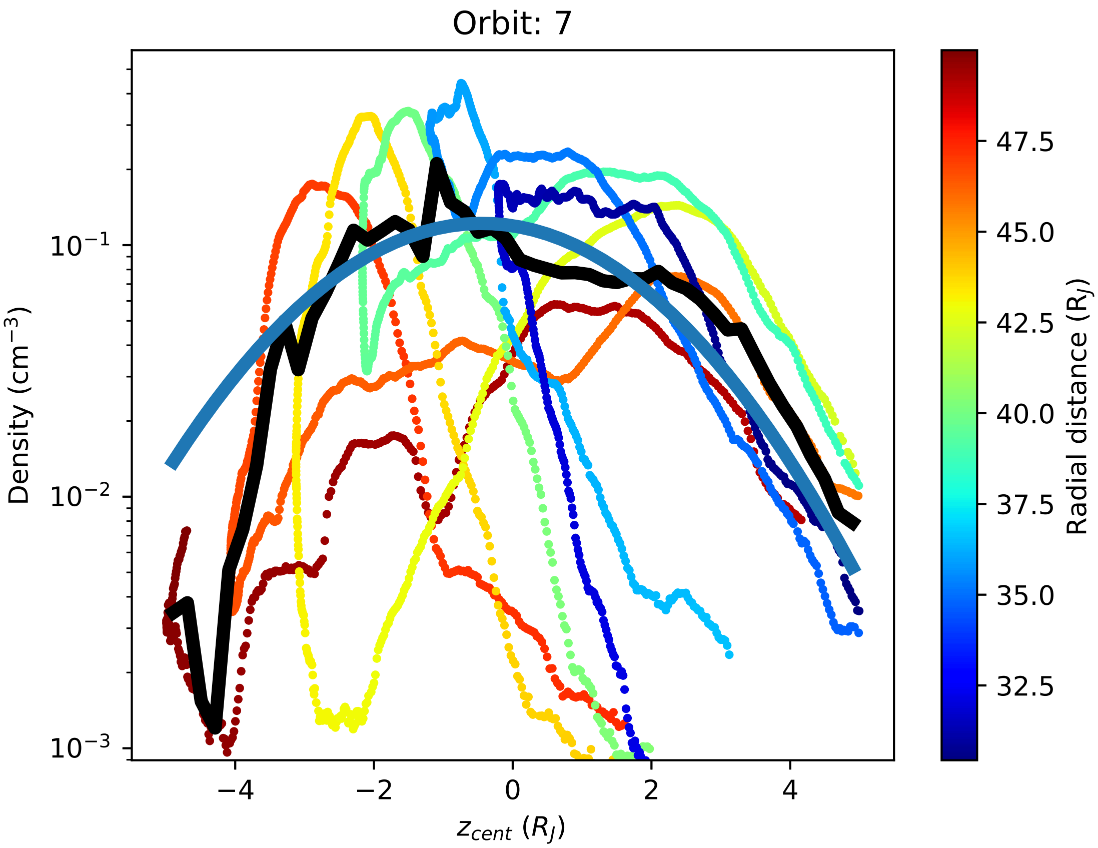

Orbit: 7
Density (cm$^{-3}$)
$10^{-1}$
$10^{-2}$
$10^{-3}$
−4
−2
0
2
4
$z_{cent}$ ($R_J$)
Radial distance ($R_J$)
47.5
45.0
42.5
40.0
37.5
35.0
32.5

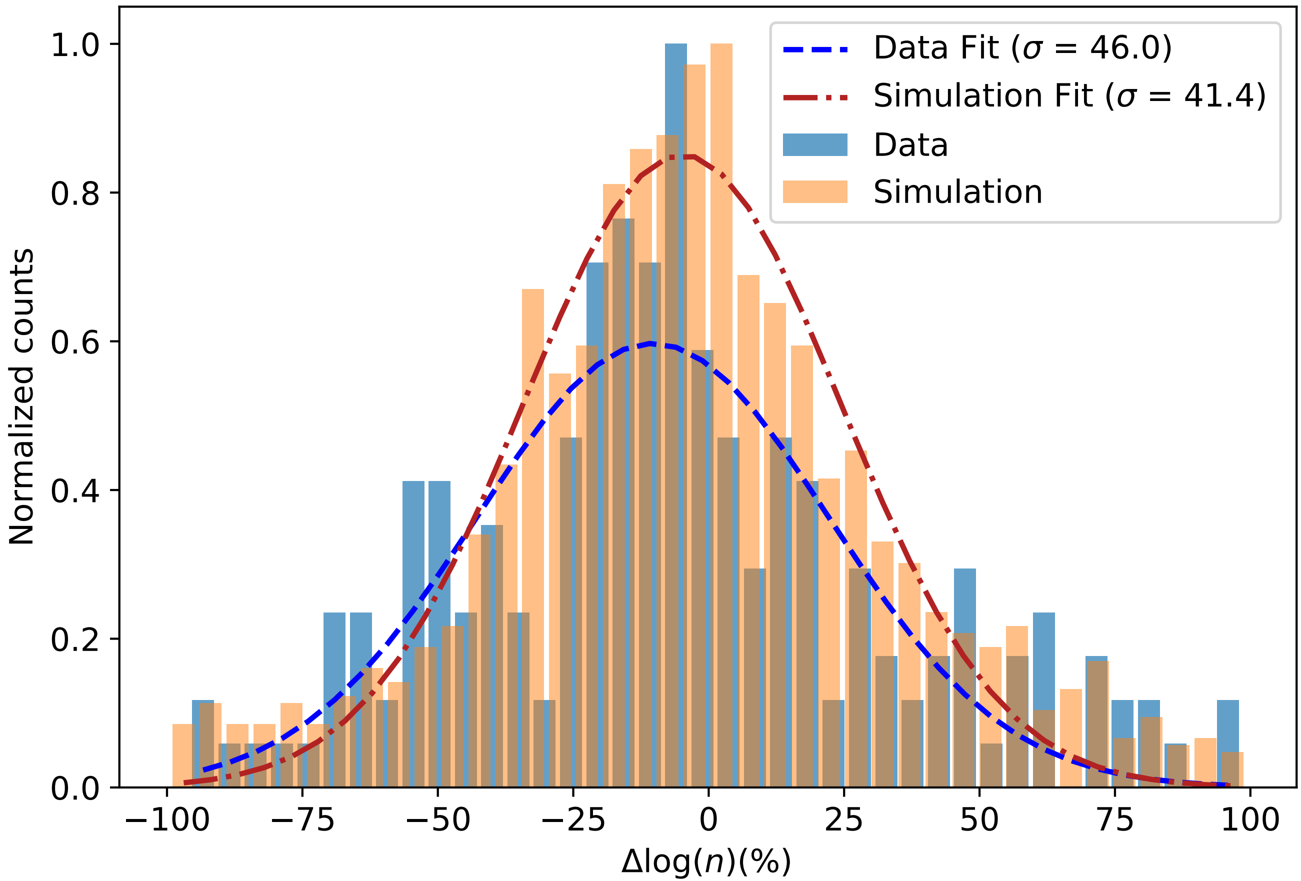
Data Fit (σ = 46.0)
Simulation Fit (σ = 41.4)
Data
Simulation
Normalized counts
Δlog(n)(%)
1.0
0.8
0.6
0.4
0.2
0.0
−100
−75
−50
−25
0
25
50
75
100

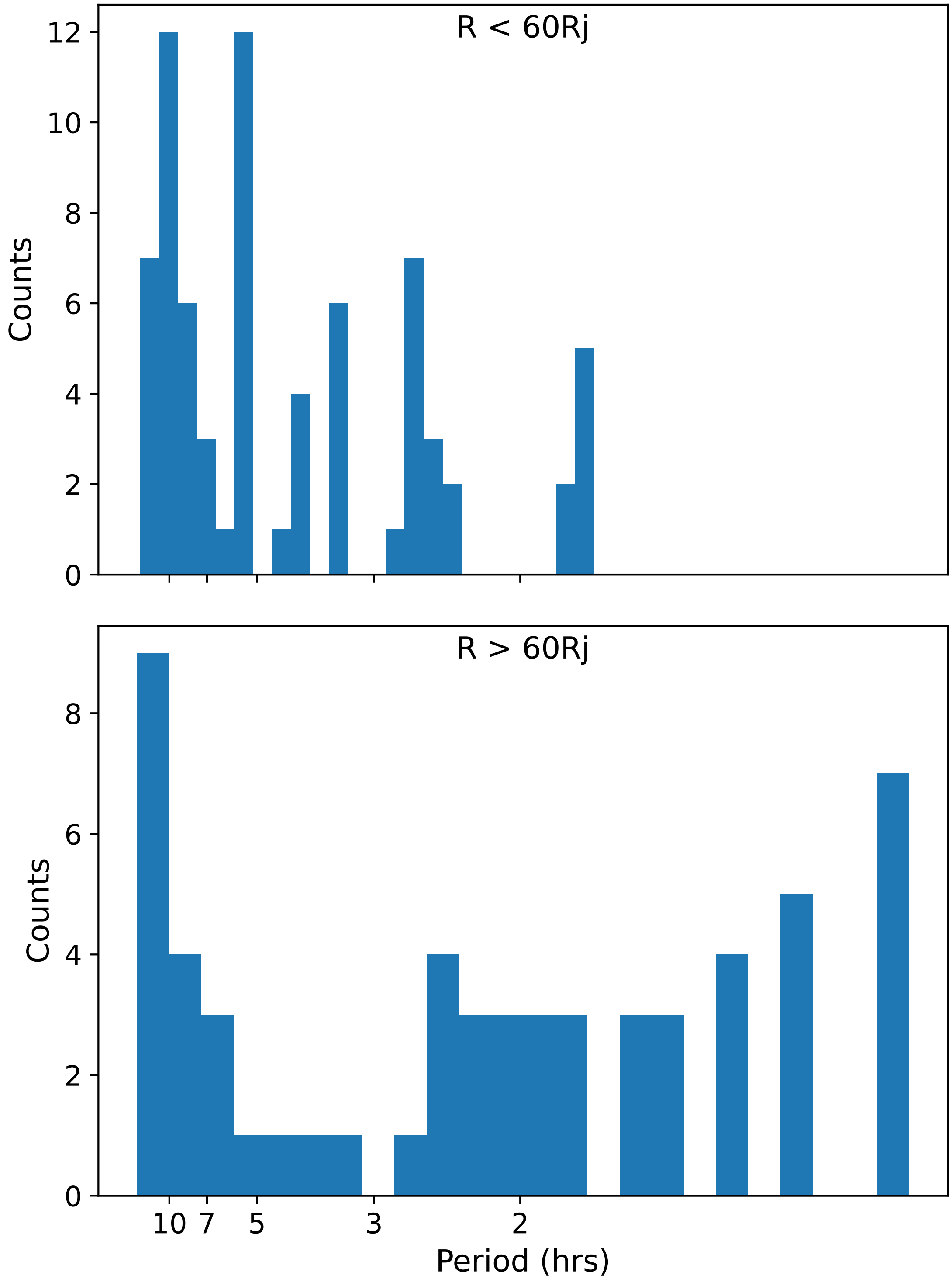
R < 60Rj
Counts
12
10
8
6
4
2
0
R > 60Rj
Counts
8
6
4
2
0
10 7 5 3 2
Period (hrs)

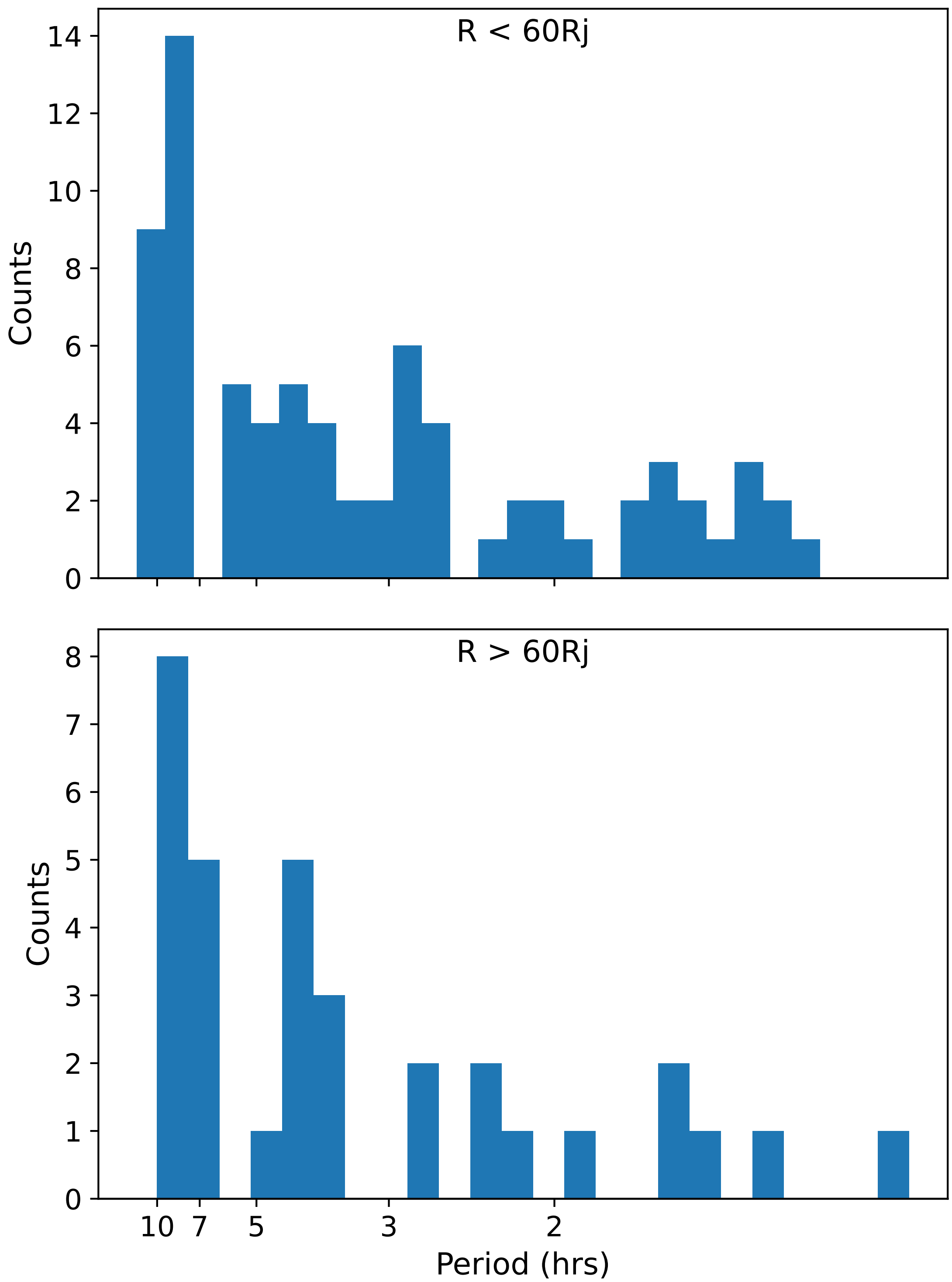
R < 60Rj
R > 60Rj
Counts
Counts
14
12
10
8
6
4
2
0
8
7
6
5
4
3
2
1
0
10
7
5
3
2
Period (hrs)